Proton-Coupled Electron Transfer in Acetonitrile Solution. Irreversible Disproportionation of $[Ru^{III}(bpy)_2(py)(OH)]^{2+}$

Robert A. Binstead,* Laura K. Stultz, and Thomas J. Meyer

Department of Chemistry, University of North Carolina at Chapel Hill, Chapel Hill, North Carolina 27599-3290

Received May 26, 1994[⊗]

The comproportionation reaction between $[Ru^{IV}(bpy)_2(py)(O)]^{2+}$ and $[Ru^{II}(bpy)_2(py)(OH_2)]^{2+}$ in acetonitrile (CH_3CN) to form 2 equiv of $[Ru^{III}(bpy)_2(py)(OH)]^{2+}$ (bpy = 2,2′-bipyridine, py = pyridine) was investigated by means of rapid-scan, stopped-flow kinetics, yielding the rate constant $k_{com} = (4.07 \pm 0.13) \times 10^3$ M^{-1} s^{-1} at 25 °C. Under the same conditions in 1% w/v H_2O or D_2O in CH_3CN the rate constants were $(3.10 \pm 0.12) \times 10^3$ M^{-1} s^{-1} and $(2.13 \pm 0.02) \times 10^2$ M^{-1} s^{-1}, respectively. The solvent isotope effect $k_{(H_2O)}/k_{(D_2O)} = 14.6 \pm 0.7$ provides evidence for proton-coupled electron transfer. The long term instability of $[Ru^{III}(bpy)_2(py)(OH)]^{2+}$ in CH_3CN was investigated by following the changes in the UV−vis spectrum over periods up to 2×10^5 s. Principal factor analysis of the spectral changes by singular value decomposition revealed the presence of four colored components during the reaction. The application of global kinetic analysis methods allowed the data to be fit to a model involving initial disproportionation to $Ru^{IV}{=}O^{2+}$ and $Ru^{II}{-}OH_2^{2+}$ ($k_{disp} = 81 \pm 8$ M^{-1} s^{-1}, 25 °C), followed by irreversible substitution of the aqua complex by CH_3CN to give $[Ru^{II}(bpy)_2(py)(NCCH_3)]^{2+}$ ($k_{solv} = (1.66 \pm 0.02) \times 10^{-3}$ s^{-1}, 25 °C). Further reaction of $Ru^{IV}{=}O^{2+}$ with solvent or impurities also occurred to give $[Ru^{II}(bpy)_2(py)(NCCH_3)]^{2+}$ ($k \sim 5 \times 10^{-6}$ s^{-1}, 25 °C). An independent study of the loss of $[Ru^{IV}(bpy)_2(py)(O)]^{2+}$ in CH_3CN revealed that $Ru^{III}{-}OH^{2+}$ was formed as an intermediate during this reaction. The rate constants from the global kinetic analysis also provided an estimate of the equilibrium constant for comproportionation, $K_{com} = 50 \pm 5$ in CH_3CN. The dependence of k_{solv} on $[H_2O]$ for solvolysis of the aqua complex by CH_3CN is consistent with a dissociative (D) mechanism. The competition ratio for capture of the 5-coordinate intermediate by H_2O or CH_3CN is $k_{AQ}/k_{AN} = 18.4 \pm 0.6$ at 25 °C.

Introduction

We have previously reported detailed mechanistic studies on the comproportionation in eq 1 in water, where $K_{com} = 72$ ($\Delta G° = 0.11$ V).[1] An unusual feature is the large H_2O/D_2O kinetic isotope effect (16.1) in either direction due to proton-coupled electron transfer. Acetonitrile has been the solvent of choice for a number of mechanistic studies involving oxidation of organic reductants by polypyridyl oxo complexes of Ru(IV) and hydroxo complexes of Ru(III).[2,3] In recent studies of epoxidation[4] or allylic oxidation[5] of alkenes by $[Ru^{IV}(bpy)_2(py)(O)]^{2+}$ and $[Ru^{IV}(tpy)(bpy)(O)]^{2+}$ complications arose from an apparent slow oxidation of CH_3CN and instability of the Ru(III) hydroxo complexes in this solvent. Here we report on the mechanism of loss of $[Ru^{III}(bpy)_2(py)(OH)]^{2+}$ in CH_3CN via initial disproportionation and further elucidation of proton-coupled electron transfer from kinetic studies of the comproportionation reaction.

$$[Ru^{IV}(bpy)_2(py)(O)]^{2+} + [Ru^{II}(bpy)_2(py)(OH_2)]^{2+} \rightleftharpoons 2[Ru^{III}(bpy)_2(py)(OH)]^{2+} \quad (1)$$

Experimental Section

Materials. High-purity acetonitrile (Burdick & Jackson) was used as the solvent for the kinetic studies without further purification. High-quality deionized water (18 MΩ) was prepared by passing house-distilled water through an E-pure (Barnstead) purification system, which included a three stage deionization process, activated charcoal removal of organic contaminants, and a final stage of microfiltration. Deuterium oxide (Aldrich, 99.9% D) was used as received. The complexes $[Ru^{II}(bpy)_2(py)(OH_2)](PF_6)_2{\cdot}H_2O$ and $[Ru^{IV}(bpy)_2(py)(O)](PF_6)_2$ were prepared and purified according to previously published procedures.[1b]

Instrumentation. UV−vis kinetic measurements for rapid reactions were made by use of an OLIS (Bogart, GA) RSM/1000 rapid-scanning, dual beam spectrophotometer attached to a Hi-Tech Scientific SF-51 stopped-flow mixing apparatus. For slower reactions UV−vis spectra were obtained as a function of time by use of a Hewlett-Packard 8452A diode array spectrophotometer with conventional or manually operated syringe mixing into standard cuvettes (NSG Precision Cells). Constant temperatures were maintained in the observation cells by use of Lauda RM6 or Neslab RTE-110 circulating baths. Temperatures were monitored via Pt resistance thermometers in both cases. Reaction mixtures were analyzed by use of a Hewlett-Packard 5890 Series II gas chromatograph with a 12 m × 0.2 mm × 0.33 μm HP-1 column (cross-linked methyl silicone gum) and a Hewlett-Packard 5971A mass selective detector, both interfaced with an HP Vectra PC computer system.

Global Kinetic Analysis. In all cases spectral-kinetic data were processed by use of the program SPECFIT (Spectrum Software Associates, Chapel Hill, NC), which is based on the published works of Zuberbühler *et al.*[6] This program uses the method of singular value decomposition (SVD) to reduce the wavelength−time spectral data matrix (**Y**) to the factor analytical form, $\mathbf{Y} = \mathbf{USV}^t$, where **U** and **V** are sets of orthogonal (linearly independent) *evolutionary* and *spectral*

[⊗] Abstract published in *Advance ACS Abstracts,* December 15, 1994.

(1) (a) Binstead, R. A.; Moyer, B. A.; Samuels, G. J.; Meyer, T. J. *J. Am. Chem. Soc.* **1981**, *103*, 2897. (b) Binstead, R. A.; Meyer, T. J. *J. Am. Chem. Soc.* **1987**, *109*, 173.
(2) (a) Moyer, B. A.; Sipe, B. K.; Meyer, T. J. *Inorg. Chem.* **1981**, *20*, 1475. (b) Roecker, L.; Dobson, J. C.; Vining, W. J.; Meyer, T. J. *Inorg. Chem.* **1987**, *26*, 779. (c) Roecker, L.; Meyer, T. J. *J. Am. Chem. Soc.* **1987**, *109*, 746. (d) Seok, W. K.; Dobson, J. C.; Meyer, T. J. *Inorg. Chem.* **1988**, *27*, 5. (e) Seok, W. K.; Meyer, T. J. *J. Am. Chem. Soc.* **1988**, *110*, 7358.
(3) Ho, C.; Che, C.-M.; Lau, T.-C. *J. Chem. Soc., Dalton Trans.* **1990**, 967.
(4) Stultz, L. K.; Binstead, R. A.; Reynolds, M. S.; Meyer, T. J. *J. Am. Chem. Soc.*, in press.
(5) Stultz, L. K.; Binstead, R. A.; Meyer, T. J. Work in progress.

0020-1669/95/1334-0546$09.00/0

eigenvectors, respectively, and **S** is a set of singular (weighting) factors. Subsequently, the eigenvectors are applied within a global multivariate least squares regression method (Levenberg–Marquardt) to fit the projection ($\mathbf{Y}' = \mathbf{US}$) of the multiwavelength kinetic data in the subspace spanned by **V** to an appropriate model for $\mathbf{Y} = \mathbf{CA}$, where the matrix **C** contains the concentration profiles and **A** represents the molar absorptivity spectra. The concentration profiles for complex kinetic systems are solved within SPECFIT by numerical integration of a user-defined set of differential rate equations. The results of such kinetic fits return both globally optimized rate constants and predicted spectra of the colored species. Where necessary, the program was used with known molar absorptivity spectra of some species in order to constrain the fit and thereby return more reliable spectra for those predicted from the fit.

In principle, there will be as many eigenvectors as there are spectra or abscissa points in each spectrum, which ever is the smaller. However, one of the advantages of the SVD is that there will be only a small number of *significant* eigenvectors containing *all* of the spectral and evolutionary information from the original set of scans. The remaining eigenvectors contain only experimental noise and can be eliminated from further consideration without loss of significant information. Purely statistical criteria for significance are not particularly useful for the determination of the number of colored components present during a reaction for several reasons. First, SVD produces successive eigenvectors with rapidly diminishing eigenvalues and some may become comparable in magnitude to experimental noise and thereby be excluded on a statistical basis. In addition, nonrandom instrumental noise may produce statistically significant eigenvectors that should not be interpreted as colored components. Such problems are more easily detected from plots of the individual eigenvectors ($\mathbf{U} \times \mathbf{S}$ *vs* time; **V** *vs* λ), which usually provide compelling evidence for the number of useful eigenvectors and those that contain only experimental noise. The identification of the number of *significant* eigenvectors is an aid in the determination of a suitable model for the data. However, this has no bearing on how many of the eigenvectors should be used for data reconstruction ($\mathbf{Y} = \mathbf{USV}^t$) during a least squares fit. The exclusion of small noise vectors is a very effective form of least squares noise filtering. Indeed, in some cases it is even possible to exclude some of the smaller *colored* eigenvectors without significantly affecting the accuracy of data reconstruction. In general, though, there is no need to take such steps since the inclusion of noise vectors has no significant effect on the fit and merely leads to somewhat larger standard deviations in the parameters.

General discussions of factor analytical methods can be found in a highly readable book by Malinowski,[7] while the subject of numerical integration of stiff differential equations is available from a number of literature sources, including the readily accessible book by Press *et al.*[8] The numerical integration routines in SPECFIT follow accepted methods for solving stiff differential kinetic systems. In cases of preequilibria or unavoidable time delays between initiation of a reaction and the first spectral measurements the numerical integration routines were used to obtain the reagent concentrations at the time of the initial observation. Where refinement of the rate constants for the initial stage of the model was required to define the starting concentrations accurately, the simulation and parameter refinements were performed repeatedly in order to obtain an acceptable fit at the first observation.

Results

Comproportionation. Absorbance–time spectral changes accompanying the formation of $[Ru^{III}(bpy)_2(py)(OH)]^{2+}$ by the comproportionation reaction between $[Ru^{IV}(bpy)_2(py)(O)]^{2+}$ and $[Ru^{II}(bpy)_2(py)(OH_2)]^{2+}$ in CH_3CN were followed by rapid-scan, stopped-flow UV–vis spectroscopy under pseudo-first-order conditions (*typically* $[Ru(IV)]_0 = 1 \times 10^{-4}$ M, $[Ru(II)]_0 = 2 \times 10^{-5}$ M, 25 °C). Owing to rapid solvolysis of $Ru^{II}-OH_2^{2+}$, the measurements were obtained with at least a 10-fold excess of $Ru^{IV}{=}O^{2+}$. Singular value decomposition of the rapid-scan spectra revealed just two significant eigenvectors, as expected for a reaction of the type $A + B \rightleftharpoons 2C$. Global least squares fits were made to a single exponential rate law in order to obtain the pseudo-first-order rate constants, k_{obs}. The reaction went to completion under these conditions allowing second-order rate constants to be derived from eq 2. This yielded an average

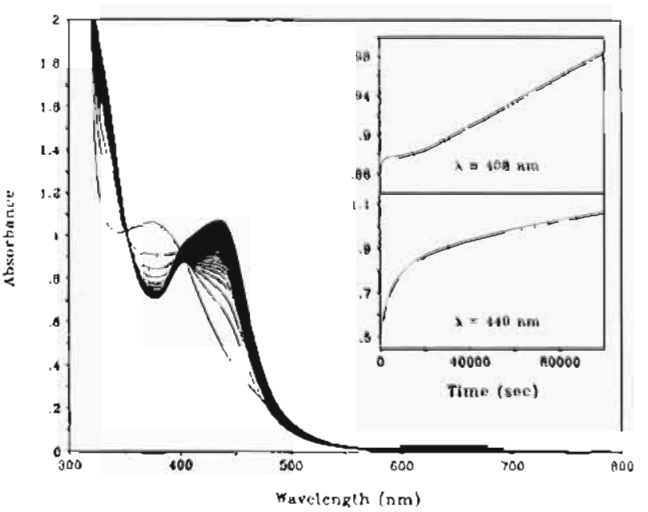

Figure 1. UV–vis spectral changes observed after mixing 1.125×10^{-4} M $[Ru^{IV}(bpy)_2(py)(O)]^{2+}$ and 1.045×10^{-4} M $[Ru^{II}(bpy)_2(py)(OH_2)]^{2+}$ in CH_3CN solution at $T = 25 \pm 0.2$ °C, shown with time steps of 3000 s between traces. (Inset: absorbance time traces for the full data set.)

$$k' = k_{obs}/[Ru(IV)]_0 \qquad (2)$$

value from 30 determinations of $k' = (4.07 \pm 0.13) \times 10^3$ M^{-1} s^{-1}, which is four times larger than the value reported previously.[2d] The value reported here has been determined independently several times from samples prepared via different synthetic routes. It is likely that the previous work was in error owing to misapplication of the stoichiometric factor of four that would apply to the reverse reaction.

Our previous studies of this reaction in aqueous media revealed a large solvent isotope effect $k_{(H_2O)}/k_{(D_2O)} = 16.1 \pm 0.2$ at 25.3 °C.[1] This work extends the investigation with studies in 1% w/v solutions of H_2O and D_2O in CH_3CN at 25 °C, returning the rate constants $k' = (3.10 \pm 0.12) \times 10^3$ M^{-1} s^{-1} and $k' = (2.13 \pm 0.02) \times 10^2$ M^{-1} s^{-1}, respectively. The small decrease in rate on addition of 1% w/v H_2O is noteworthy since in pure H_2O the rate constant is 1 order of magnitude higher, $k' = (4.46 \pm 0.03) \times 10^4$ M^{-1} s^{-1} at 25.3 °C.[1] However, the kinetic isotope effect of 14.6 ± 0.7 in this medium is essentially unchanged from that observed in water.

Disproportionation. The disappearance of $[Ru^{III}(bpy)_2(py)(OH)]^{2+}$ in CH_3CN was followed by UV–vis spectrophotometry as a function of time, as illustrated in Figure 1. Singular value decomposition of the collected spectra returned nine sets of eigenvectors. As illustrated in Figure 2, just four of these contained significant colorimetric information related to the reaction. The fifth spectral eigenvector (**V**) was consistent with the line spectrum of the deuterium lamp source of the HP 8452A diode array spectrophotometer, and the corresponding temporal changes ($\mathbf{U} \times \mathbf{S}$) most likely arise from changes in lamp intensity. The remaining eigenvectors contained only random noise that could be factored from the data. During the initial stage of the reaction there was discernible spectral evidence for

(6) (a) Gampp, H.; Maeder, M.; Meyer, C. J.; Zuberbühler, A. D. *Talanta* **1985**, *32*, 95. (b) Gampp, H.; Maeder, M.; Meyer, C. J.; Zuberbühler, A. D. *Talanta* **1985**, *32*, 257. (c) Maeder, M.; Zuberbühler, A. D. *Anal. Chem.* **1990**, *62*, 2220.

(7) Malinowski, E. R. *Factor Analysis in Chemistry*, 2nd ed.; Wiley-Interscience: New York, 1991.

(8) Press, W. H. *Numerical Recipes in FORTRAN*; Cambridge University Press: New York, 1992.

(9) Doppelt, P.; Meyer, T. J. *Inorg. Chem.* **1987**, *26*, 2027.

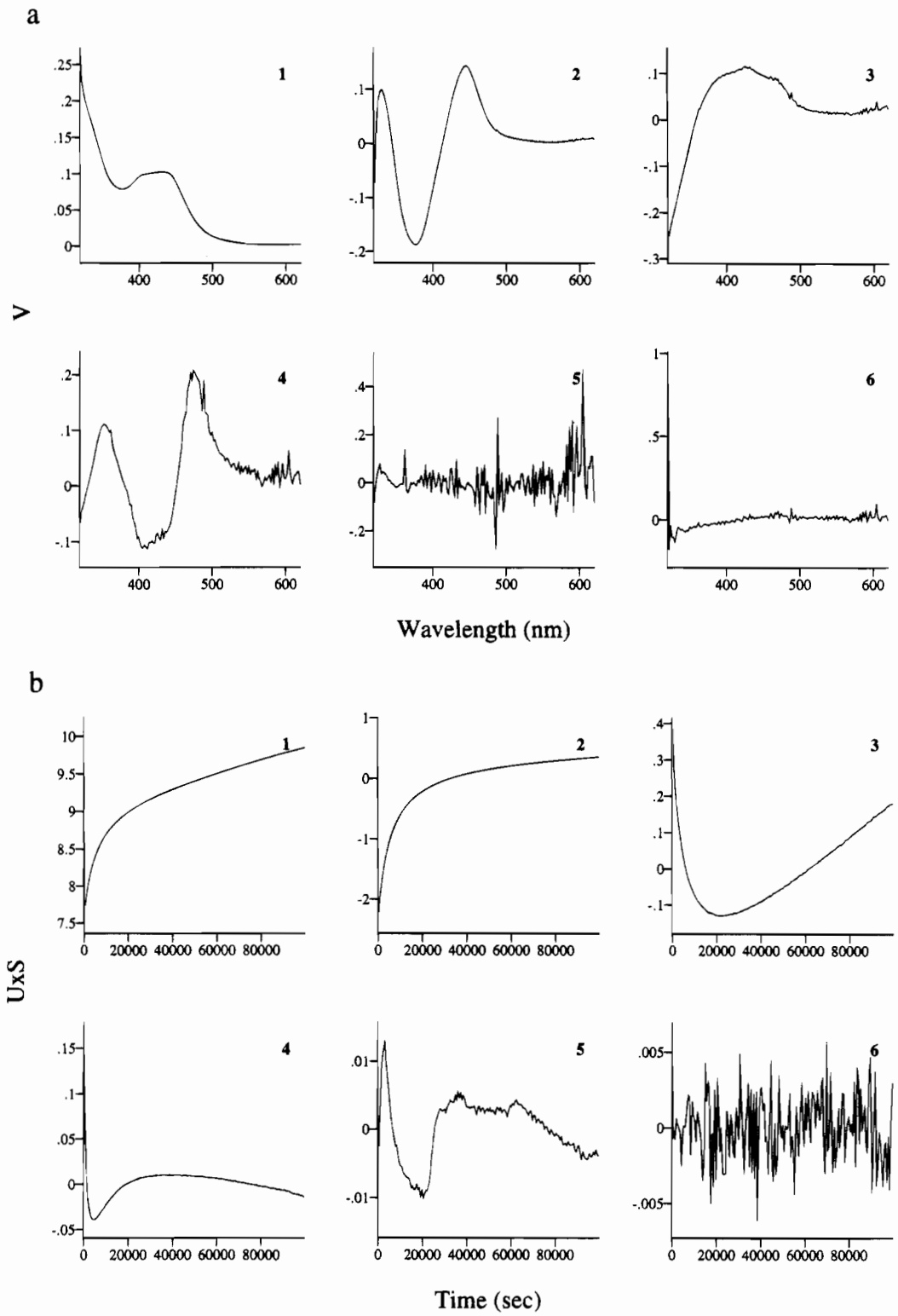

Figure 2. Singular value decomposition of the spectral-kinetic data matrix **Y** in Figure 1 for the decomposition of $[Ru^{III}(bpy)_2(py)(OH)]^{2+}$ in CH_3CN solution at $T = 25 \pm 0.2$ °C showing (a) the first six spectral eigenvectors **V** and (b) the first six temporal eigenvectors from **U** × **S**.

the presence of a small, equilibrium fraction of $[Ru^{II}(bpy)_2(py)(OH_2)]^{2+}$ ($\lambda_{max} \sim 470$ nm). This spectral feature disappeared within a few minutes with concomitant formation of the solvento complex, $[Ru^{II}(bpy)_2(py)(NCCH_3)]^{2+}$ ($\lambda_{max} = 440$ nm). However, $Ru^{II}-NCCH_3^{2+}$ continued to grow on a much slower time scale, with approximately 50% formation occurring in 24 h. There was little evidence for the formation of the μ-oxo-bridged dimer $[(bpy)_2(py)Ru^{III}-O-Ru^{III}(bpy)_2(py)]^{4+}$ ($\lambda_{max} \sim 640$ nm) on this time scale.[9] The remaining oxidative equivalents were quenched rapidly by the addition of solid hydroquinone directly to the observation cell, yielding initially $Ru^{II}-OH_2^{2+}$, followed by quantitative recovery of $Ru^{II}-NCCH_3^{2+}$.

Solvolysis. The solvolysis of $[Ru^{II}(bpy)_2(py)(OH_2)]^{2+}$ (1×10^{-4} M) was studied independently at 25 °C after dissolution of the PF_6^- salt in CH_3CN containing 1×10^{-5} M hydroquinone to reduce any $Ru^{III}-OH^{2+}$ impurity present in the sample (*typically* 1%). Singular value decomposition of the data set revealed just two significant eigenvectors, as expected for a simple A → B reaction, and a subsequent global fit of the data to a single exponential rate law returned the first-order rate constant, $k = (1.655 \pm 0.001) \times 10^{-3}$ s^{-1}. On the basis of extrapolation to $t = 0$, the global analysis also returned the pure spectrum of $Ru^{II}-OH_2^{2+}$ ($\lambda_{max} = 468$ nm, $\epsilon = 8750$ M^{-1} cm^{-1}) in CH_3CN as well as that of $Ru^{II}-NCCH_3^{2+}$ ($\lambda_{max} = 440$ nm,

Table 1. Solvolysis of $[Ru^{II}(bpy)_2(py)(OH_2)]^{2+}$ in CH_3CN/H_2O Solutions at 25 ± 0.2 °C

% H_2O (w/v)	$[H_2O]$, M	10^3k_{obs}, s^{-1} [a]	% H_2O (w/v)	$[H_2O]$, M	10^3k_{obs}, s^{-1} [a]
0.00	0.000	1.655	1.50	0.834	0.917
0.31	0.172	1.408	2.00	1.11	0.793
0.61	0.339	1.239	4.00	2.22	0.539
1.00	0.555	1.096	10.00	5.55	0.335

[a] The standard errors from global fits were typically ±0.1%, but the reproducibility was only ~1%.

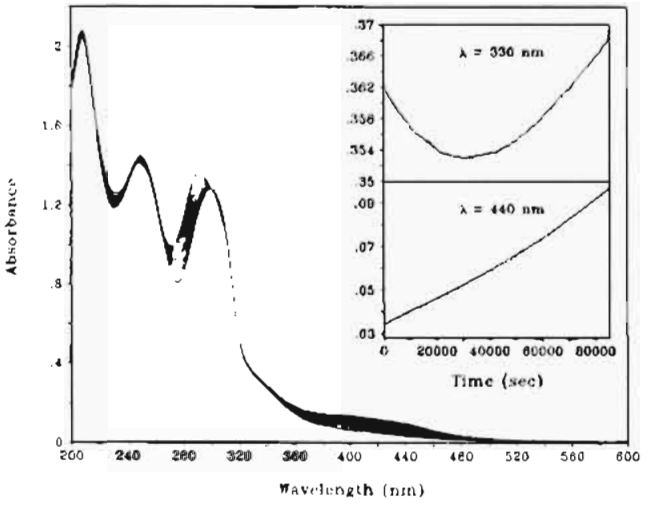

Figure 3. UV−vis spectral changes observed after dissolving 5.67 × 10^{-5} M $[Ru^{IV}(bpy)_2(py)(O)]^{2+}$ in CH_3CN solution at T = 25 ± 0.2 °C, shown with time steps of 7500 s between traces. (Inset: absorbance time traces for the full data set.)

ϵ = 8160 M^{-1} cm^{-1}). The spectrum of the aqua complex obtained from the global fit is very similar to that observed in water (λ_{max} = 472 nm, ϵ = 8800 M^{-1} cm^{-1}).[1b] The effect of added H_2O on the rate of solvolysis was investigated over the range 0−10% w/v H_2O/CH_3CN at 25 °C. The results of the global fits for single determinations are collected in Table 1. The standard deviations obtained from the global fits were very small (±0.1%), owing to both the excellent adherence to first-order behavior and the statistical weight of many simultaneous observations. However, replicate measurements were reproducible to only ±1%, presumably as a result of small temperature variations from run to run.

Decomposition. The results above suggest that the equilibrium (1) is also maintained in CH_3CN solution, but solvolysis of the aqua complex results in irreversible loss of Ru(III), yielding $Ru^{IV}{=}O^{2+}$ and $Ru^{II}{-}NCCH_3^{2+}$. However, the solvento complex continues to be formed (>50% recovery) over a period of several days. This suggests that another pathways exists for the loss of $Ru^{IV}{=}O^{2+}$ via oxidation of the solvent or impurities contained therein. A separate study was undertaken to follow the loss of $[Ru^{IV}(bpy)_2(py)(O)]^{2+}$ in CH_3CN, as shown in Figure 3 for measurements obtained over a 24 h period. The reaction proved to be very slow and was not followed to completion. Singular value decomposition of the collected spectra revealed just three significant eigenvectors. In this case, no spectral evidence of the aqua complex would be expected owing to the relative rapidity of solvolysis on the time scale of the decomposition reaction.

An attempt was made to determine the products from the reduction of $[Ru^{IV}(bpy)_2(py)(O)]^{2+}$ in CH_3CN by allowing a 20 mM sample of $Ru^{IV}{=}O^{2+}$ to react at room temperature, protected from light, for 3 days. The UV−vis spectrum of this mixture revealed that the complex products were $Ru^{II}{-}NCCH_3^{2+}$ and a small fraction (<2%) of the μ-oxo-bridged dimer $[(bpy)_2(py)Ru^{III}{-}O{-}Ru^{III}(bpy)_2(py)]^{4+}$. GC−MS analysis revealed small amounts of water and propionitrile at the same levels in the solvent and reaction mixture with no detectable organic products from oxidation of the solvent or impurities therein. It is possible that the large solvent peak obscured such products if they were formed.

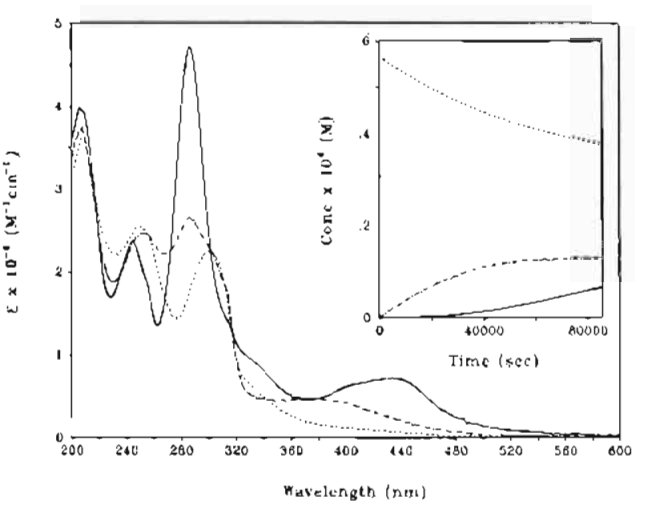

Figure 4. Predicted UV−vis molar absorptivity spectra for $[Ru^{IV}(bpy)_2(py)(O)]^{2+}$ (- - -), $[Ru^{III}(bpy)_2(py)(OH)]^{2+}$ (− • −), and $[Ru^{II}(bpy)_2(py)(NCCH_3)]^{2+}$ (—) in CH_3CN solution at T = 25.0 ± 0.2 °C obtained from the decomposition of $[Ru^{IV}(bpy)_2(py)(O)]^{2+}$. (Inset: concentration profiles obtained from the global fit to the kinetic model given in the text.)

Kinetic Model. A single kinetic model was used to fit the disappearances of both $[Ru^{III}(bpy)_2(py)(OH)]^{2+}$ and $[Ru^{IV}(bpy)_2(py)(O)]^{2+}$ in CH_3CN. The available data suggest that the reactions in eq 3 explain the decomposition chemistry, with the

$$2[Ru^{III}(bpy)_2(py)(OH)]^{2+} \underset{k_1}{\overset{k_{-1}}{\rightleftharpoons}} [Ru^{IV}(bpy)_2(py)(O)]^{2+} + [Ru^{II}(bpy)_2(py)(OH_2)]^{2+} \quad (3a)$$

$$[Ru^{II}(bpy)_2(py)(OH_2)]^{2+} + CH_3CN \xrightarrow{k_2} [Ru^{II}(bpy)_2(py)(NCCH_3)]^{2+} + H_2O \quad (3b)$$

$$[Ru^{IV}(bpy)_2(py)(O)]^{2+} + CH_3CN \xrightarrow{k_3} [Ru^{III}(bpy)_2(py)(OH)]^{2+} + \text{unknown products} \quad (3c)$$

assumption of a pseudo-first-order reaction for the loss of $Ru^{IV}{=}O^{2+}$. The global fits were constrained by use of known values for k_1 and k_2, which were determined independently (see above). For decomposition of $[Ru^{IV}(bpy)_2(py)(O)]^{2+}$, a fixed value k_{-1} = 81 M^{-1} s^{-1} was used while k_3 was optimized. The value of k_{-1} was determined from global fits of the spectral data for disappearance of $[Ru^{III}(bpy)_2(py)(OH)]^{2+}$. In the latter case, k_1, k_2, and k_3 were held fixed initially while k_{-1} was allowed to vary. This procedure converged rapidly to self-consistent values of k_{-1} and k_3.

The global fit for decomposition of $Ru^{IV}{=}O^{2+}$ returned k_3 = 6.7 × 10^{-6} s^{-1}. The predicted spectra and concentration profiles for the three colored species present are shown in Figure 4. These remarkable results confirm that $Ru^{III}{-}OH^{2+}$ is an intermediate present during the course of the decomposition chemistry and that $Ru^{II}{-}NCCH_3^{2+}$ is the final product. The absolute molar absorptivity values for the predicted spectrum of $[Ru^{II}(bpy)_2(py)(NCCH_3)]^{2+}$ are about 10% lower than expected, but this is not unreasonable considering the small extent (~30%) of reaction observed. Reanalysis of the data

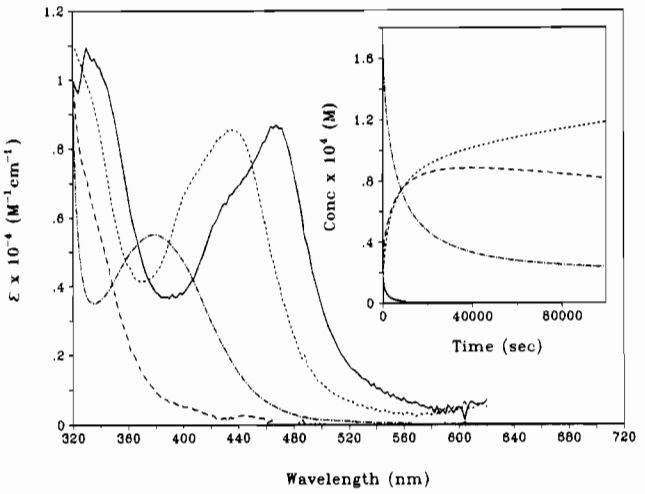

Figure 5. Predicted UV−vis molar absorptivity spectra for $[Ru^{IV}(bpy)_2(py)(O)]^{2+}$ (− − −), $[Ru^{III}(bpy)_2(py)(OH)]^{2+}$ (− • −), $[Ru^{II}(bpy)_2(py)(OH_2)]^{2+}$ (—), and $[Ru^{II}(bpy)_2(py)(NCCH_3)]^{2+}$ (- - -) in CH_3CN solution at $T = 25.0 \pm 0.2$ °C obtained from the disproportionation of $[Ru^{III}(bpy)_2(py)(OH)]^{2+}$. (Inset: concentration profiles obtained from the global fit to the kinetic model given in the text.)

with use of the known molar absorptivity spectrum of $Ru^{II}-NCCH_3^{2+}$ as a further constraint gave $k_3 = 5.7 \times 10^{-6}$ s^{-1}.

The global fit for the disappearance of $Ru^{III}-OH^{2+}$ was complicated by the low relative concentration of $Ru^{II}-OH_2^{2+}$ during the course of the reaction, leading to a somewhat noisy, inaccurate predicted spectrum for this species. Therefore, the wavelength range was limited in order to avoid noisy regions and the fit was constrained with use of the known spectrum of the aqua complex. Reanalysis returned the optimized rate constants $k_{-1} = (80.6 \pm 0.4)$ M^{-1} s^{-1} and $k_3 = (4.6 \pm 0.1) \times 10^{-6}$ s^{-1}. On the basis of global fits to multiple data sets obtained on different time scales (5×10^4−2×10^5 s), the accuracy of these rate constants is estimated to be no better than approximately ±10% and ±20%, respectively. The spectral predictions and concentration profiles from the constrained global fit are shown in Figure 5. The predicted spectrum of $Ru^{II}-NCCH_3^{2+}$ is about 5% higher than expected, its accuracy being limited ultimately by the inability to follow the reaction to completion. The residuals surface for the global fit revealed slight misfit (~1%) at the beginning of the reaction arising from errors in analytical concentrations and a number of sharp spectral features related to variations in the deuterium lamp source with time. Otherwise the deviations between the data and fit were very small, as shown in Figure 6.

One of the interesting results obtained from the global analysis is the availability of a predicted spectrum of $Ru^{III}-OH^{2+}$ in CH_3CN ($\lambda_{max} = 380$ nm, $\epsilon = 5520$ M^{-1} cm^{-1}), a result that cannot be achieved experimentally. Another important result is the ability to determine the value of the comproportionation equilibrium constant, $K_{com} = k_1/k_{-1}$, from the globally fitted rate constants for the model. These give an approximate value of $K_{com} = 50 \pm 5$ in CH_3CN, which is close to the value of $K_{com} = 72$ observed in water. This is consistent with spectral observations that reveal the presence of small, equilibrium amounts of $Ru^{II}-OH_2^{2+}$ during the early stages of the disproportionation of $Ru^{III}-OH^{2+}$. However, the rapid solvolysis of the aqua complex had frustrated attempts to measure the equilibrium constant directly from the initial spectra.

Discussion

The results of this study explain the origins of the long term instability of $[Ru^{III}(bpy)_2(py)(OH)]^{2+}$ in CH_3CN in terms of the mechanism shown in eq 3. The initial disproportionation is thermodynamically unfavorable but the reaction is driven by the irreversible substitution of $Ru^{II}-OH_2^{2+}$ by CH_3CN to give $Ru^{II}-NCCH_3^{2+}$ and $Ru^{IV}=O^{2+}$. The final step is the slow reaction of $Ru^{IV}=O^{2+}$ with solvent or impurities therein. The

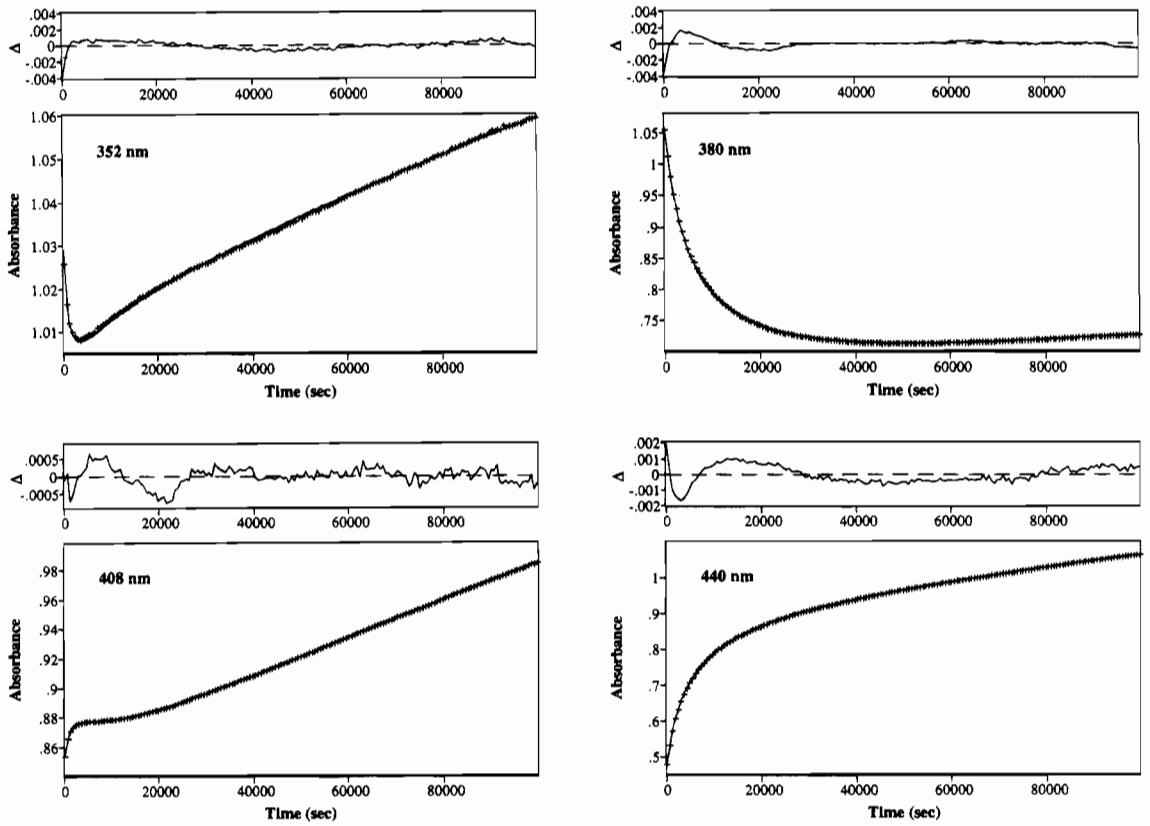

Figure 6. Single wavelength comparisons of the data (+), fit (—), and residuals trace (Δ) from the global fit to the kinetic model given in the text for disproportionation of $[Ru^{III}(bpy)_2(py)(OH)]^{2+}$ in CH_3CN solution at $T = 25.0 \pm 0.2$ °C.

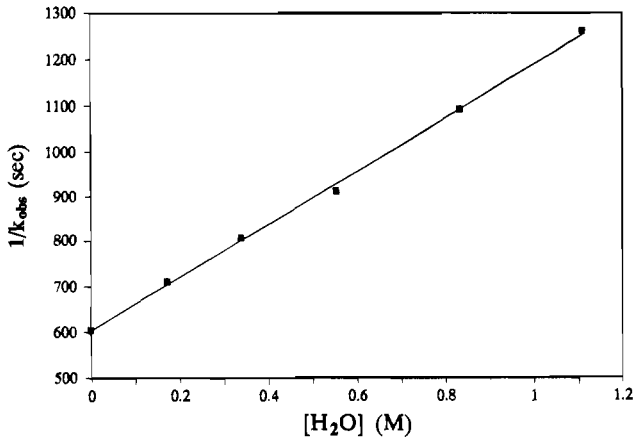

Figure 7. Water dependence on the rate of solvolysis of $[Ru^{II}(bpy)_2(py)(OH_2)]^{2+}$ in CH_3CN solution at $T = 25.0 \pm 0.2$ °C, plotted as $1/k_{obs}$ *vs* $[H_2O]$.

appearance of $Ru^{III}-OH^{2+}$ as an intermediate during the decomposition of $Ru^{IV}=O^{2+}$ supports this. The final product is predominantly $Ru^{II}-NCCH_3^{2+}$ with a small amount of the μ-oxo-bridged dimer (Figure 1). The mechanism for its appearance is unknown.

Substitution of $Ru^{II}-OH_2^{2+}$ by CH_3CN. The observed rate law for substitution of the aqua ligand by CH_3CN is consistent with a dissociative (D) mechanism (eq 4) in its dependence on

$$[Ru^{II}(bpy)_2(py)(OH_2)]^{2+} \underset{k_{-d}}{\overset{k_d}{\rightleftharpoons}} [Ru^{II}(bpy)_2(py)]^{2+} + H_2O \quad (4a)$$

$$[Ru^{II}(bpy)_2(py)]^{2+} + CH_3CN \xrightarrow{k_s} [Ru^{II}(bpy)_2(py)(NCCH_3)]^{2+} \quad (4b)$$

added H_2O. Assuming that the steady state approximation holds for the 5-coordinate intermediate, the observed rate constant, k_{obs}, is predicted to vary with added water according to eq 5

$$k_{obs} = \frac{k_d k_s}{k_{-d}[H_2O] + k_s} \quad (5)$$

under conditions where $[H_2O] \ll [CH_3CN]$. A plot of $1/k_{obs}$ *vs* $[H_2O]$, with slope $= k_{-d}/(k_d k_s)$ and intercept $= 1/k_d$, is shown in Figure 7. The linearity is maintained up to 2% w/v (1.11 M) H_2O. At higher concentrations of H_2O there is increasing departure from linearity since $k_s = k_s'$ $[CH_3CN]$ is no longer constant. A linear least squares fit of the data up to 2% w/v H_2O gives $k_d = (1.66 \pm 0.02) \times 10^{-3}$ s^{-1} ($r = 0.9994$) and the ratio $k_{-d}/k_s = 0.97 \pm 0.03$. Given the concentration of pure CH_3CN = 18.9 M at 25 °C, this indicates that there is a significant kinetic preference (18.4 ± 0.6) for the coordination of H_2O over CH_3CN. This is a remarkable observation since $Ru^{II}-NCCH_3^{2+}$ is the thermodynamically preferred product and is completely formed even in 50% w/v H_2O/CH_3CN. The kinetic preference for H_2O and its effect on the distribution between $Ru^{II}-NCCH_3^{2+}$ and $Ru^{II}-OH_2^{2+}$ has implications for catalysis since formation of the aqua complex is required for re-entry into the $Ru^{IV}=O^{2+}/Ru^{III}-OH^{2+}/Ru^{II}-OH_2^{2+}$ redox system either by chemical or electrochemical oxidation.

Proton-Coupled Electron Transfer. The reaction between $Ru^{IV}=O^{2+}$ and $Ru^{II}-OH_2^{2+}$ in CH_3CN is important in a mechanistic sense in what it reveals about proton-coupled electron transfer. The addition of 1% w/v H_2O to CH_3CN does not appear to affect the kinetics appreciably, the slight reduction of 25% in the observed rate constant being attributable to changes in driving force or solvent reorganizational energy. The change in rate constant is not a colligative property since k_{com} in pure water is 1 order of magnitude higher.[1] The observation of $k_{(H_2O)}/k_{(D_2O)} = 14.6 \pm 0.7$ at 25 °C is comparable to the isotope effect of 16.1 ± 0.2 in water, where electrochemical measurements have been used to establish that $\Delta G°$ is the same in H_2O and D_2O.[1] Reasonable mechanisms for comproportionation are

(a) initial outer-sphere electron transfer followed by H^+ transfer:

$$Ru^{IV}=O^{2+} + Ru^{II}-OH_2^{2+} \rightarrow Ru^{III}-O^+ + Ru^{III}-OH_2^{3+}$$

$$Ru^{III}-O^+ + Ru^{III}-OH_2^{3+} \rightarrow Ru^{III}-OH^{2+} + Ru^{III}-OH^{2+}$$

(b) initial H^+ transfer followed by outer-sphere electron transfer:

$$Ru^{IV}=O^{2+} + Ru^{II}-OH_2^{2+} \rightarrow Ru^{IV}=OH^{3+} + Ru^{II}-OH^+$$

$$Ru^{IV}=OH^{3+} + Ru^{II}-OH^+ \rightarrow Ru^{III}-OH^{2+} + Ru^{III}-OH^{2+}$$

(c) simultaneous H^+/e^- transfer:

$$Ru^{IV}=O^{2+} + Ru^{II}-OH_2^{2+} \rightarrow Ru^{III}-OH^{2+} + Ru^{III}-OH^{2+}$$

In water, the first two pathways can be ruled out on thermodynamic grounds.[1b] The large difference between the first pK_a values for $Ru^{II}-OH_2^{2+}$ (10.3) and $Ru^{III}-OH_2^{3+}$ (0.85) and the low affinity of $Ru^{IV}=O^{2+}$ for protons ($pK_a < 0$) result in free energy changes for the initial steps that exceed the experimental free energy of activation, $\Delta G^{\ddagger} < \Delta G°$.[1b] The available spectroscopic evidence is consistent with similar acidities for the aqua ligands in CH_3CN solution. This, combined with the large $k_{(H_2O)}/k_{(D_2O)}$ isotope effect, points to the likelihood of the synchronous mechanism (c) involving *simultaneous* transfer of both a proton and an electron from $Ru^{II}-OH_2^{2+}$ to $Ru^{IV}=O^{2+}$,

$$(bpy)_2(py)Ru^{IV}=O^{2+}, H(OH)-Ru^{II}(bpy)_2(py)^{2+} \rightarrow (bpy)_2(py)Ru^{III}-OH^{2+}, HO-Ru^{III}(bpy)_2(py)^{2+}$$

This occurs within an association complex, specifically oriented to facilitate the coupled electron–proton transfer event. This mechanism is more complex than either initial outer-sphere electron transfer or initial proton transfer, since there must be coordinate dependent electron–vibrational coupling along the ν_{OH} coordinate as the reaction proceeds. A more complete understanding awaits a quantum mechanical analysis, including electron–vibrational coupling and the electronic influence of spin–orbit coupling.

Acknowledgment. This work was supported by the National Science Foundation under Grant No. CHE-9203311. The authors also express their appreciation to Prof. Andreas D. Zuberbühler at the University of Basel for access to the global least squares algorithms used in the development of the SPECFIT program and for continuing advice on the application of factor analytical methods to kinetic systems.

IC940600X